

## ON THE EQUILIBRIUM OF A DISTORTED HETEROGENEOUS ELLIPSOIDAL MASS. III: THE HETEROGENEOUS SPHEROIDAL MASS

J. U. Cisneros Parra,<sup>1</sup> F. J. Martínez Herrera,<sup>2</sup> and J. D. Montalvo Castro<sup>2</sup>

Received June 24 2016; accepted July 5 2016

### RESUMEN

En nuestro trabajo I empleamos, de manera aproximada, el teorema de Bernoulli para estudiar el equilibrio de un esferoide homogéneo deformado auto-gravitante, con corrientes internas de vorticidad diferencial donde, por comodidad, se supuso que la constante  $k$  de esa ecuación era la misma en todas partes del cuerpo, lo que eventualmente condujo a inconsistencias, que desaparecieron al permitir que cada línea de corriente tenga su propia  $k$ . En el presente trabajo investigamos, mediante una ley de rotación simple y precisa, el equilibrio de un cuerpo heterogéneo que consiste de dos esferoides deformados concéntricos -núcleo y envoltura- cuyos semiejes no guardan relación alguna entre sí. El modelo aporta, para cada valor de la densidad relativa del cuerpo, series pentaparamétricas de figuras, restringidas por ciertos límites geométricos y físicos. La distribución de velocidad angular pertinente es por cilindros coaxiales al eje de rotación; contrariamente a lo estipulado en nuestro trabajo II, la distribución por discos no es posible.

### ABSTRACT

In our Paper I, Bernoulli's theorem was employed in an approximate form to study the equilibrium of a self-gravitating homogeneous distorted spheroid, with internal differential vorticity currents, where, for ease, the Bernoulli constant  $k$  was taken as being the same everywhere, eventually leading this to inconsistencies, which are no longer present when each streamline has its own  $k$ . In the current paper we investigate, through a simple and general rotation law, the equilibrium of a heterogeneous body composed of two concentric distorted spheroids—core and envelope—whose axes are not correlated. The model yields, for each value of the body's relative density, five-parametric series of figures, constrained by certain geometrical and physical limits. The pertinent distribution for the angular velocity is by cylinders coaxial with the rotation axis. Contrary to what was stated in our Paper II, the distribution by disks is impossible.

*Key Words:* gravitation — hydrodynamics — stars: rotation

### 1. INTRODUCTION

In Cisneros et al. I (2015) equilibrium figures were obtained from a self-gravitating homogeneous liquid mass endowed with an internal motion of differential vorticity, whose surface equation was that of either a distorted ellipsoid or a distorted spheroid; however, as we noticed *a posteriori*, the figures, called ellipsoidal and spheroidal after Jeans (1920), were erroneously deduced, although their qualitative features remained more or less unaffected (see § 5.1).

<sup>1</sup>Facultad de Ciencias, Universidad Autónoma de San Luis Potosí, México.

<sup>2</sup>Instituto de Física, Universidad Autónoma de San Luis Potosí, México.

In the current paper, we investigate the equilibrium of a heterogeneous model consisting of two concentric homogeneous spheroidal masses of different density, the 'nucleus' and the 'atmosphere' (whose semi-axes are not correlated) through a simple and precise rotation law. Affixing sub indexes  $n$  and  $a$  to the pertinent quantities, the body's relative density,  $(\rho_n - \rho_a)/\rho_a$ , is denoted by  $\varepsilon$ , with  $\rho_n > \rho_a$ , so that the distribution of density is somewhat closer to that prevailing in real stars. The quantities in our development are normalized as explained in Cisneros et al. I (2015).

## 2. BERNOULLI'S THEOREM, THE CLASSICAL HOMOGENEOUS FIGURES AND OURS

Before going on with our heterogeneous model, we wish to discuss Bernoulli's theorem as is commonly employed for obtaining the classical homogeneous figures (Lyttleton 1953; Dryden 1956), particularly the Dedekind ellipsoids which, along with our models, are static. The steady-state equations of motion for a self-gravitating fluid are

$$(\mathbf{v} \cdot \text{grad})\mathbf{v} = \text{grad } V - \frac{1}{\rho} \text{grad } p, \quad \text{div } \mathbf{v} = 0, \quad (1)$$

where  $\mathbf{v}$  is the velocity field,  $V$  is the potential and  $p$  is the pressure. These equations can also be written as

$$\text{grad} \left( \frac{1}{2} \mathbf{v}^2 - V + \frac{1}{\rho} p \right) = \mathbf{v} \times (\text{rot } \mathbf{v}), \quad \text{div } \mathbf{v} = 0. \quad (2)$$

For a streamline (tangent to  $\mathbf{v}$ ) we get, after taking the dot product of  $\mathbf{v}$  in the first equation (2),

$$\mathbf{v} \cdot \text{grad} \left( \frac{1}{2} \mathbf{v}^2 - V + \frac{1}{\rho} p \right) = 0; \quad (3)$$

that is

$$\frac{1}{2} \mathbf{v}^2 - V + \frac{1}{\rho} p = k, \quad (4)$$

$k$  being constant on a streamline. Commonly,  $k$  changes from one streamline to another, being an overall constant only when  $\text{rot } \mathbf{v} = 0$ . The changes in  $k$  are dictated by [cf. equations (2) and (4)]

$$\text{grad } k = \mathbf{v} \times (\text{rot } \mathbf{v}). \quad (5)$$

The Maclaurin and Jacobi figures are characterized by the rotational velocity field

$$\mathbf{v} = \omega (-y, x, 0), \quad (6)$$

where  $\omega$  is the constant angular velocity. We can see that relation (6) satisfies the continuity equation  $\text{div } \mathbf{v} = 0$ . According to equation (6), the  $k$  in Bernoulli's equation is given by

$$\text{grad } k = 2\omega^2(x, y, 0), \quad (7)$$

that is

$$\frac{\partial k}{\partial x} = 2\omega^2 x, \quad \frac{\partial k}{\partial y} = 2\omega^2 y, \quad \frac{\partial k}{\partial z} = 0, \quad (8)$$

from which we deduce

$$k = \omega^2(x^2 + y^2) + c, \quad (9)$$

$c$  being any constant. Therefore, Bernoulli's equation (4) becomes

$$-\frac{1}{2}\omega^2(x^2 + y^2) - V + \frac{1}{\rho} p = c, \quad (10)$$

which agrees with the well-known equation.<sup>3</sup>

While the Jacobi and the Maclaurin figures rotate as a rigid body, a Dedekind ellipsoid ( $1, e_2, e_3$  are the major, middle, and minor semi-axes) remains fixed in space, its equilibrium being due to an internal motion of uniform vorticity  $\zeta$ , its velocity field being

$$\mathbf{v} = \frac{\zeta}{1 + e_2^2} (-y, e_2^2 x, 0). \quad (11)$$

We can convince ourselves that  $\mathbf{v}$  is tangent to ellipses  $x^2 + y^2/e_2^2 = \text{const.}$ . Hence, streamlines are ellipses perpendicular to the  $z$ -axis. For  $\zeta$  constant, the velocity field satisfies the continuity equation, and  $k$  obeys the relation

$$\text{grad } k = \frac{\zeta^2}{1 + e_2^2} (e_2^2 x, y, 0), \quad (12)$$

so that

$$\frac{\partial k}{\partial x} = \frac{\zeta^2}{1 + e_2^2} e_2^2 x, \quad \frac{\partial k}{\partial y} = \frac{\zeta^2}{1 + e_2^2} y, \quad \frac{\partial k}{\partial z} = 0. \quad (13)$$

The solution of the partial differential equations (13) is

$$k = \frac{\zeta^2}{2(1 + e_2^2)} (e_2^2 x^2 + y^2) + c, \quad (14)$$

where  $c$  is an arbitrary constant. In this case, Bernoulli's equation

$$\frac{\zeta^2}{2(e_2^2 + 1)^2} (e_2^4 x^2 + y^2) - V + p = \frac{\zeta^2}{2(1 + e_2^2)} (e_2^2 x^2 + y^2) + c,$$

reduces to

$$-V - \frac{e_2^2 \zeta^2}{2(e_2^2 + 1)^2} (x^2 + y^2) + \frac{1}{\rho} p = c. \quad (15)$$

This is essentially equation (10) for obtaining the Jacobi ellipsoids if we put

$$\omega^2 = \frac{\zeta^2 e_2^2}{2(e_2^2 + 1)^2}, \quad (16)$$

a known result that establishes the equivalence between Jacobi's angular velocity and Dedekind's vorticity (Chandrasekhar 1969). Of course, if we had assumed from the beginning that  $k = \text{const.}$ , it would have been impossible to reach equation (15).

<sup>3</sup>Lyttleton assumes from the beginning that  $k$  is constant; he obtains a valid result because of the special value of  $k$  of the present case.

2.1. *General Case with Cylindrical Symmetry*

Each fluid point rotates, now, with non-constant angular velocity  $\omega$ . The velocity field is given again by

$$\mathbf{v} = \omega (-y, x, 0), \tag{17}$$

but the continuity equation leads, presently, to

$$\operatorname{div} \mathbf{v} = -y \frac{\partial \omega}{\partial x} + x \frac{\partial \omega}{\partial y} = 0,$$

or

$$\frac{\partial \omega}{\partial x^2} = \frac{\partial \omega}{\partial y^2}, \tag{18}$$

which means that, generally, the angular velocity must be a function of the kind

$$\omega = \omega (x^2 + y^2, z). \tag{19}$$

Assuming, additionally, that the velocity field is symmetric about the  $z$ -axis, we can express it as

$$\omega = \omega (x^2 + y^2, z^2). \tag{20}$$

Here, it is more convenient to use cylindrical coordinates  $(R, \varphi, z)$ , and so the problem is independent of one coordinate:  $\varphi$ . In this system, the velocity field (tangent to circles) has a  $\varphi$ -component alone:

$$\mathbf{v} = \omega (0, R, 0). \tag{21}$$

Equation (5) will have two terms only:

$$\frac{\partial k}{\partial R^2} = \omega \left( R^2 \frac{\partial \omega}{\partial R^2} + \omega \right), \quad \frac{\partial k}{\partial z^2} = R^2 \omega \frac{\partial \omega}{\partial z^2}. \tag{22}$$

Making the variable change

$$\omega = \sqrt{\frac{2\Omega}{R^2}}, \tag{23}$$

equations (22) become

$$\frac{\partial k}{\partial R^2} = \frac{\partial \Omega}{\partial R^2} + \frac{1}{R^2} \Omega, \quad \frac{\partial k}{\partial z^2} = \frac{\partial \Omega}{\partial z^2}. \tag{24}$$

From the last of equations (24), we deduce

$$k (R^2, z^2) = \Omega (R^2, z^2) + f (R^2), \tag{25}$$

where  $f$  is an arbitrary function. Therefore, the first equation (24) implies that

$$\Omega (R^2, z^2) = R^2 f' (R^2),$$

or

$$\omega^2 = 2 f' (R^2), \tag{26}$$

i. e., the angular velocity can be at most a function of  $R$  alone, and the same for  $k$ :

$$k = R^2 f' (R^2) + f (R^2) = \frac{1}{2} R^2 \omega^2 + f (R^2). \tag{27}$$

In other words, the angular velocity distribution has cylindrical symmetry. Since  $k$  does not depend exclusively on  $z$ , disk-like distributions are impossible, contrary to what we stated in Paper II. Substituting  $k$  of equation (27) into Bernoulli's equation (4), we obtain

$$-f (R^2) - V (R^2, z^2) + \frac{1}{\rho} p = 0. \tag{28}$$

Since the function  $f$  depends on  $R$  but not on  $z$  (i. e., it is constant on cylinders), we can determine it using only the surface equation, on which  $p = 0$ :

$$f (R^2) = -V (R^2, z^2), \tag{29}$$

where  $z$  is a function of  $R$  for a figure with cylindrical symmetry. Equation (29) allows to determine the function  $f (= -V)$ , and with equation (26)  $\omega$  is established:

$$\omega^2 = -2 \frac{dV}{dR^2}, \tag{30}$$

which is the general angular velocity distribution law for any axial-symmetric, incompressible, self-gravitating fluid with  $p = 0$  on its surface. Equation (30) is, essentially, Newton's second law for a unit mass particle:

$$(\text{Radial force}) \frac{dV}{dR} = -\omega^2 R (= \text{centripetal acceleration}).$$

Using the familiar variable  $r (= x^2 + y^2 = R^2)$ , equation (30) can be written as

$$\omega^2 = -2 \frac{dV}{dr}. \tag{31}$$

In the special case of a Maclaurin spheroid, the potential can be expressed as

$$V = v_c - v_1 (x^2 + y^2) - v_3 z^2 = v_c - v_1 r - v_3 z^2.$$

At any interior point; on the surface ( $r + z^2/e_3^2 = 1$ ), we have

$$V = v_c - v_3 e_3^2 + (v_3 e_3^2 - v_1) r.$$

Hence, according to equation (31), the angular velocity is given by

$$\omega^2 = 2 (v_1 - v_3 e_3^2),$$

which agrees with the well-known result. Taking into account that

$$v_3 = \frac{2\pi \left( -e_3^2 - e_3 \sqrt{1 - e_3^2} \cos^{-1}(e_3) + 1 \right)}{(1 - e_3^2)^2},$$

and that  $v_1 = 2\pi - v_3$ , we can also write

$$\omega^2 = \frac{2\pi e_3 \left( 3e_3 \sqrt{1 - e_3^2} - (2e_3^2 + 1) \cos^{-1}(e_3) \right)}{(1 - e_3^2)^{3/2}}.$$

## 2.2. The Homogeneous Spheroidal Mass

The surface equation of the homogeneous spheroidal mass (the ellipsoidal mass will not be considered here) is

$$x^2 + y^2 + \frac{z^2}{e_3^2} + d \frac{z^4}{e_3^4} = 1, \quad (32)$$

where  $d$  is a parameter larger than  $-1/4$ ; the rotation semi-axis is not  $e_3$ , but

$$z_M = e_3 \sqrt{\frac{\sqrt{4d+1} - 1}{2d}}. \quad (33)$$

For establishing the angular velocity at equilibrium (31), we must take the derivative of the potential with respect to  $r$  at the surface. Since  $V$  is only known numerically, this process has to be carried out numerically. Nonetheless, we can use another approach. We approximate the potential by a polynomial in  $r$  of the form

$$V = \alpha_0 + \alpha_1 r + \alpha_2 r^2 + \alpha_3 r^3 + \alpha_4 r^4, \quad (34)$$

so that the angular velocity becomes

$$\omega^2 = -2(\alpha_1 + 2\alpha_2 r + 3\alpha_3 r^2 + 4\alpha_4 r^3). \quad (35)$$

For  $d$  not too large, the mean absolute error in  $V$  is about  $10^{-7}$ , which grows with increasing  $d$  (for  $d = 2$ , the mean error is  $10^{-4}$ ).

## 3. THE HETEROGENEOUS SPHEROIDAL MASS

The composite model consists of a core, or nucleus, of density  $\rho_n$ , whose shape is

$$\frac{x^2 + y^2}{e_1^2} + \frac{z^2}{e_n^2} + d_n \frac{z^4}{e_n^4} = 1, \quad (36)$$

surrounded by an envelope, or atmosphere, of density  $\rho_a$ , of the form

$$x^2 + y^2 + \frac{z^2}{e_a^2} + d_a \frac{z^4}{e_a^4} = 1. \quad (37)$$

Here  $e_1$  is the ratio of the nucleus and atmosphere major axes;  $e_n$  and  $e_a$  are proportional to the rotation semi-axes, which are

$$z_{Mn} = e_n \sqrt{\frac{\sqrt{4d_n+1} - 1}{2d_n}}, \quad z_{Ma} = e_a \sqrt{\frac{\sqrt{4d_a+1} - 1}{2d_a}}. \quad (38)$$

The net potentials at any point of the nucleus and the atmosphere are (Montalvo et al. 1983),

$$V_N = \varepsilon V_{nn} + V_{na}, \quad V_A = \varepsilon V_{an} + V_{aa}, \quad (39)$$

respectively, where  $V_{nn}$  is the self-potential of the nucleus;  $V_{na}$  is the potential on the nucleus due to the atmosphere;  $V_{an}$  is the potential on the atmosphere due to the nucleus;  $V_{aa}$  is the self-potential of the atmosphere;  $\varepsilon$  is the body's relative density difference:

$$\varepsilon = \frac{\rho_n - \rho_a}{\rho_a}. \quad (40)$$

Let us now suppose that core and envelope rotate with (variable) angular velocities  $\omega_n$  and  $\omega_a$ , so that their velocity fields are

$$\mathbf{v}_n = \omega_n (-y, x, 0), \quad \mathbf{v}_a = \omega_a (-y, x, 0). \quad (41)$$

Both fields must obey the continuity equation  $\text{div } \mathbf{v} = 0$ . Thus, according to equation (20), we have

$$\omega_n = \omega_n (x^2 + y^2, z^2), \quad \omega_a = \omega_a (x^2 + y^2, z^2). \quad (42)$$

In the equilibrium state the angular velocities (42) must fulfill Bernoulli's equation:

$$\frac{p}{\rho_n} = V_N + f_n(R^2), \quad \frac{p}{\rho_a} = V_A + f_a(R^2), \quad (43)$$

where  $f_n$  and  $f_a$  are functions to be determined.  $f_n$  and  $f_a$  are established from the surface conditions  $p_n = p_a$  (core surface) and  $p_a = 0$  (envelope surface), where  $p_n$  and  $p_a$  are pressures on points of the nucleus and the atmosphere:

$$\varepsilon V_N + (1 + \varepsilon) f_n(R^2) - f_a(R^2) = 0, \quad V_A + f_a(R^2) = 0. \quad (44)$$

Using equation (31), these relations can be written as

$$\omega_a^2 = -2 \frac{dV_A}{dr}, \quad \omega_n^2 = -\frac{2\varepsilon}{1 + \varepsilon} \frac{dV_N}{dr} + \frac{1}{1 + \varepsilon} \omega_a^2, \quad (45)$$

where  $r = x^2 + y^2$  and  $V_N$ ,  $V_A$  are potentials on core and envelope surfaces, taken as functions of  $r$  only. Thus, for establishing  $\omega_a$  and  $\omega_n$ , the potential derivatives must be available at each point of the surface. Since the potential is given numerically,

its derivative must be numerically computed. For a homogeneous body (only interior points are needed), we find that a reasonable good approximated expression for the potential at points on the surface is:

$$V = \alpha_0 + \alpha_1 r + \alpha_2 r^2 + \alpha_3 r^3 + \alpha_4 r^4, \quad (46)$$

where  $\alpha_i$  are parameters to be fixed by fit procedures, and thus the angular velocity is given by equation (35)

In the case of our heterogeneous mass, equation (46) is not acceptable, especially at points where external potentials are needed (they must approach 0, as  $r \rightarrow \infty$ ). To obtain equilibrium figures for the heterogeneous case, the potential derivatives will be established by numerical means. For this purpose, we use the approximation

$$f'(r) = \frac{f(r+h) - f(r-h)}{2h}, \quad (47)$$

where  $h$  is a small quantity. The precision of expression (47) is of order  $h^2$ . A not too small value for  $h$  will be used, since potentials are calculated with an accuracy of about  $10^{-7}$ ; a reasonable  $h$  could be  $\approx 5 \times 10^{-3}$ .

#### 4. MODEL GEOMETRY

The heterogeneous mass can easily be built by making the two surfaces similar: coordinates of corresponding surface points are proportional, so that

$$\frac{x^2 + y^2}{e_1^2} + \frac{z^2}{e_n^2} + d_n \frac{z^4}{e_n^4} = c^2 \left( x^2 + y^2 + \frac{z^2}{e_a^2} + d_a c^2 \frac{z^4}{e_a^4} \right), \quad (48)$$

for all  $(x, y, z)$ , from what it follows that  $c = 1/e_1$ ,  $e_n = e_1 e_a$  and  $d_n = d_a$ . Thus, the whole mass is characterized by only two parameters, say,  $e_a$  and  $d_a$  (and, of course, the relative size  $e_1$  of major semi-axes, and the relative density difference  $\varepsilon$ ). Hence, the series, should they exist, would be relatively simple to handle. Yet we prefer to explore a more general case, and let  $e_n, e_a, d_n, d_a$  vary freely, thus leading to more involved series (actually, six-parametric, if we take into account the parameters  $e_1$  and  $\varepsilon$ ). The model effectively yields series which are subject to certain limits, both physical and geometrical; for instance, the major semi-axis of the atmosphere must be greater than that of the nucleus:  $e_1 < 1$ ; besides, the rotation semi-axes  $z_{Mn}, z_{Ma}$  must be smaller than the corresponding major semi-axes:

$$z_{Mn} < e_1, \quad z_{Ma} < 1,$$

or [cf. equation (38)]

$$e_n < e_1 \sqrt{\frac{2d_n}{\sqrt{4d_n+1}-1}}, \quad e_a < \sqrt{\frac{2d_a}{\sqrt{4d_a+1}-1}}. \quad (49)$$

Finally, the rotation semi-axis of the atmosphere must not be smaller than that of the nucleus, otherwise the atmosphere would intrude in the nucleus, and the present equilibrium conditions would not apply:

$$z_{Ma} > z_{Mn}. \quad (50)$$

The particular configuration for which  $z_{Mn} = z_{Ma}$  ( $e_1 \neq 1$ ), i. e., when the poles coincide, is termed a ‘contact figure’;  $e_a$  and  $e_n$  are related by

$$e_a = e_n \sqrt{\frac{d_a (\sqrt{4d_n+1}-1)}{d_n (\sqrt{4d_a+1}-1)}}. \quad (51)$$

### 5. NUMERICAL RESULTS

#### 5.1. The Homogeneous Spheroidal Mass

Clearly, our calculations of (Cisneros et al. 2015, Paper I) must be affected if the right  $k$  in Bernoulli’s equation (4) is used, but the qualitative features of the new figures remain more or less alike. In the case of homogeneous figures for which the surface equation is

$$x^2 + y^2 + \frac{z^2}{e_3^2} + d \frac{z^4}{e_3^4} = 1,$$

we come as before to continuous  $e_3$ -series for each  $d$  value and, furthermore, we again find limits. For  $d$  positive, and low  $e_3$ -values up to a definite limit,  $\omega^2$  increases from pole to equator; thereafter, the tendency is inverted (Figure 1). For  $d$  negative (but greater than  $-1/4$ ), another limit appears: as  $d$  becomes more and more negative, the  $e_3$ -series becomes shorter, because  $\omega^2$  takes negative values, and the figures come into a forbidden region (Figure 1), a behavior that was also noticed in previous work.

#### 5.2. The Heterogeneous Spheroidal Mass

The present series are more involved than those for the homogeneous case, so we must proceed carefully and not try to get an overwhelming bulk of models that would render it difficult to give a clear panorama of their regularities. For this purpose, a basic series is constructed by fixing five parameters:  $\varepsilon = 1$ ,  $e_1 = 0.5$ ,  $e_n = 0.1$  and  $d_n = d_a = -1/8$ , while the remaining one  $e_a$  is let to vary in its allowed range.

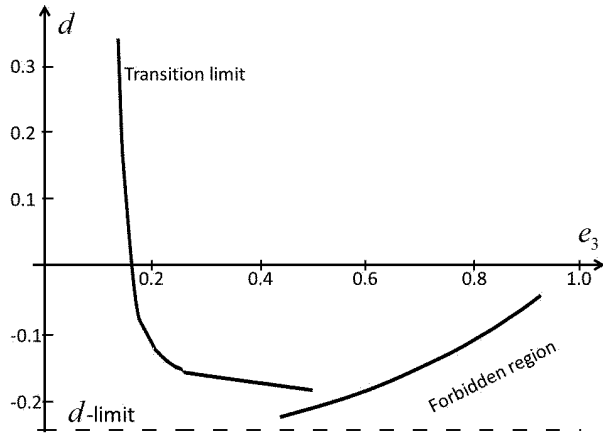


Fig. 1. Limiting  $e_3$ - $d$  curves for the  $\omega^2$  tendency transition (left) and the forbidden region (right) where  $\omega^2$  is partially negative. In fact, the last figure is plotted from the condition that  $\omega^2$  is 0 at the pole.

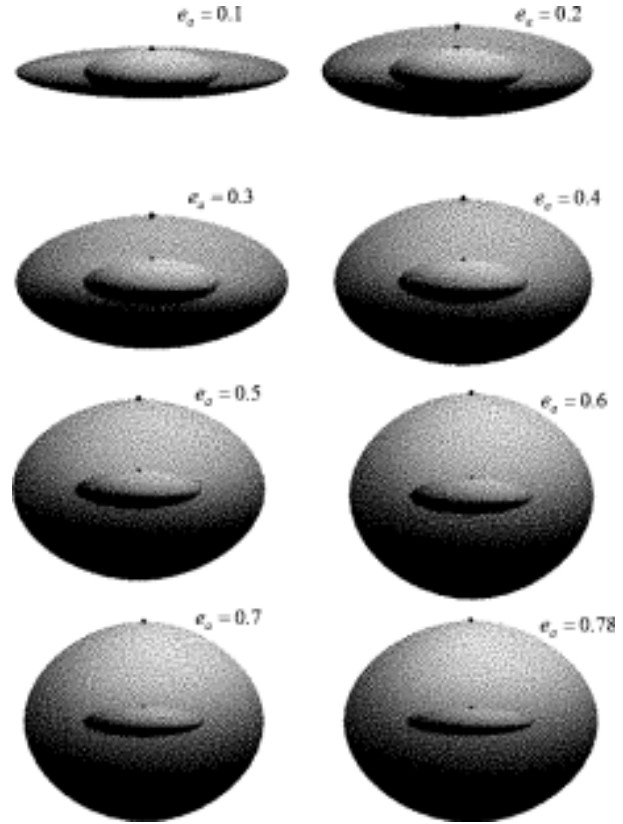


Fig. 3. Heterogeneous equilibrium figures as  $e_a$  varies from 0.1 (contact figure) to the limiting value 0.78. Poles are suggested by a thick dot. Fixed parameters are:  $e_1 = 0.5$ ,  $e_n = 0.1$ ,  $d_a = d_n = -1/8$ ,  $\varepsilon = 1$ .

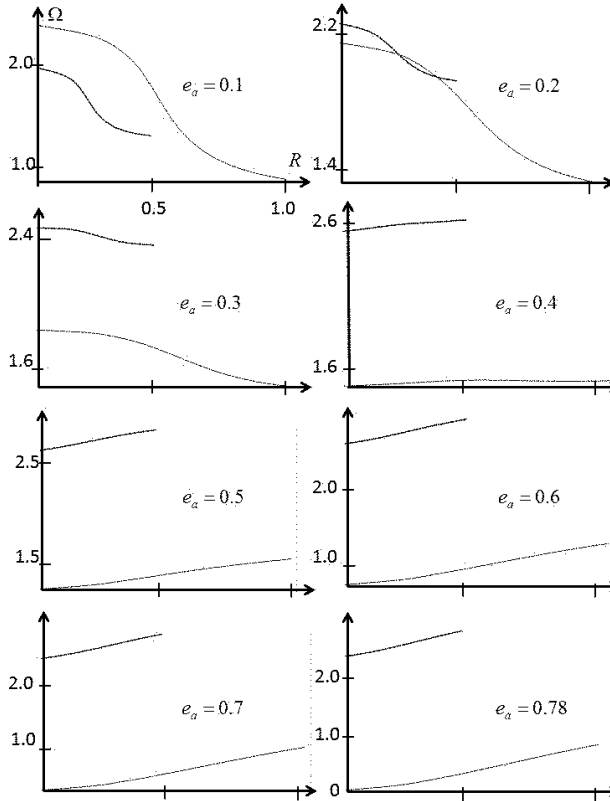


Fig. 2. Angular velocity distribution between pole ( $R = 0$ ) and equator for the nucleus (shorter line) and atmosphere as  $e_a$  varies from 0.1 (contact figure) to the limiting value 0.78. Fixed parameters are:  $e_1 = 0.5$ ,  $e_n = 0.1$ ,  $d_n = d_a = -1/8$ ,  $\varepsilon = 1$ .

5.2.1. The Case  $d_n = d_a = -1/8$

First, we take  $d_n = d_a = -1/8$  and allow  $e_a$  to vary from 0.1 up to its maximum value, finding that equilibrium is possible for the angular velocity distribution given by equation (31) for the envelope and core. In Figure 2 we plot the angular velocity distribution in the nucleus ( $R < 0.5$ ), and the atmosphere ( $R < 1$ ); Figure 3 is a sketch of the model geometry.

In Figure 2 (see also Figure 3), the series begins with a contact figure in which the poles of core and envelope touch each other, but not the equators, since the equator of the atmosphere is twice as large as that of the nucleus ( $e_1 = 0.5$ ). We see that the core rotates slower than its envelope, even at the pole. In both, the angular velocity decreases from pole to equator, i. e., the central parts rotate faster than the outer ones. As  $e_a$  increases (the atmosphere expands),  $\omega_a^2$  decreases, until a point is reached where the tendency is reversed: the angular velocity now increases from pole to equator, remain-

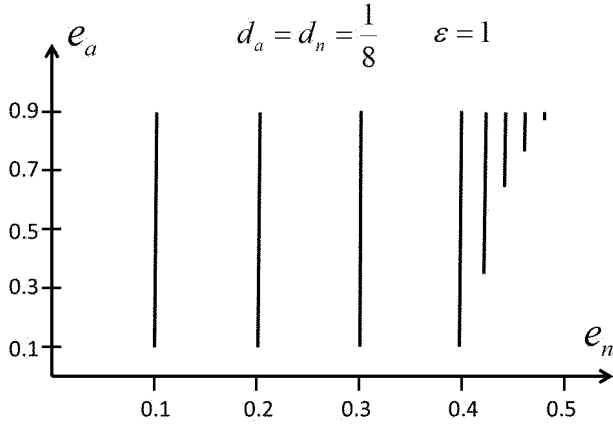


Fig. 4. Sketch of  $e_n$ -series for  $d_a = d_n = 1/8, \varepsilon = 1$ . The series begin with a contact figure for  $e_n < 0.3975$  and end at an  $e_a$  around 0.9. After  $e_n = 0.3975$  they become narrower and begin without a contact figure.

ing so up to the end; we say that a transition figure occurs. For larger  $e_a$ -values,  $\omega_a^2$  steadily decreases, reaching a zero value at the pole; thereafter, it is negative and unacceptable. The limit is achieved at  $e_a = 0.78$  ( $z_{Ma} = 0.84$ ). At the same time, less dramatic changes in the core occur with increasing  $e_a$ : the pole  $\omega_n^2$  increases a little, until the angular velocity decreasing tendency ends: a transition figure occurs. Subsequently,  $\omega_n^2$  monotonically increases from pole to equator. Both angular velocity distributions have, therefore, two limits: one for which  $\omega^2$  becomes zero at a point, and the other, less drastic, where the angular velocity reverses its tendency from monotonically decreasing to increasing. Certainly, the change takes place gradually, and we refer to a limit when  $\omega^2$  increases monotonically for the first time. Still another limit might be disclosed by building more series for larger  $e_n$  values. Indeed, we find similar series starting with a contact figure and ending up with a top figure ( $e_a \approx 0.78$ ) if  $e_n \leq 0.3975$  ( $z_{Mn} = 0.43$ ). For the small interval  $0.4004 > e_n > 0.3975$  there are series that do not begin with a contact figure and end with a one-member series at  $e_n = 0.4004, e_a = 0.969$ .

5.2.2. The Case  $d_n = d_a = 1/8$

Here we take  $d_n = d_a = 1/8$  and let  $e_a$  vary from 0.1 (contact figure) up. Once more, we get a set of series somewhat different from the former one (Figure 2), but also sharing several properties:

1. The series begins with a contact figure with the atmosphere rotating faster than the nucleus, as formerly.

2. Both differential angular velocities always monotonically decrease from pole to equator. In other words, there are not transition figures.
3. The limiting figure occurs at  $e_a = 0.967$  ( $z_{Ma} = 0.917$ ).
4. The contact figure has a limit for  $e_n = 0.398$  (cf. § 2.1.1).
5. The series do not end at  $e_n = 0.398$ ; they continue for larger  $e_n$  and are more and more narrow, ending with an isolated figure with  $e_n = 0.4827, e_a = 0.969$  ( $z_{Mn} = 0.457$ ) (see Figure 4).

Hence, the plus sign of  $d_a, d_n$  hinders the monotonous property of the angular velocity, and raises the upper limit of  $e_a$ . Additionally, the series does not disappear after a last contact figure, but at a higher  $e_n$  limit.

5.2.3. The Case  $d_n = 1/8, d_a = -1/8$

This time, only  $d_n$  sign is modified, so that our set of parameters is

$$e_1 = \frac{1}{2}, \quad e_n = \frac{1}{10}, \quad d_n = \frac{1}{8}, \quad d_a = -\frac{1}{8}, \quad \varepsilon = 1.$$

Once more, the series starts with the contact figure  $e_a = 0.0876$ ;  $e_a$  is established by  $z_{Ma} = z_{Mn}$  condition (equation (51)). The series resembles more the  $d_a = d_n = -1/8$  case than the  $d_a = d_n = 1/8$  one, in the sense that it has angular velocity transition limits and a limiting contact figure at  $e_n \approx 0.4$  ( $z_{Mn} = 0.38$ ). For greater  $e_n$  values, there are, however, more series without an initial contact figure, which become narrower as  $e_n \rightarrow 0.5$  ( $z_{Mn} = 0.47$ ). For  $e_n = 0.5$  there only exists a series with the member  $e_a = 0.97$  ( $z_{Ma} = 0.92$ ).

5.2.4. The Case  $d_n = -1/8, d_a = 1/8$

Here,  $d_a$  alone is modified relative to first case, so that the parameters values are now

$$e_1 = \frac{1}{2}, \quad e_n = -\frac{1}{10}, \quad d_n = -\frac{1}{8}, \quad d_a = \frac{1}{8}, \quad \varepsilon = 1.$$

With these parameters, we also establish series starting with a contact figure, when  $e_n < 0.4$  ( $z_{Mn} = 0.43$ ). Series without a contact figure are possible when  $0.4 < e_n < 0.421$ ; for  $e_n = 0.421$  ( $z_{Mn} = 0.46$ ) the series has a unique member at  $e_a = 0.97$ . The atmosphere does not present angular velocity transition limits, and the nucleus has only one, at  $e_n = 0.2, e_a = 0.6$ .

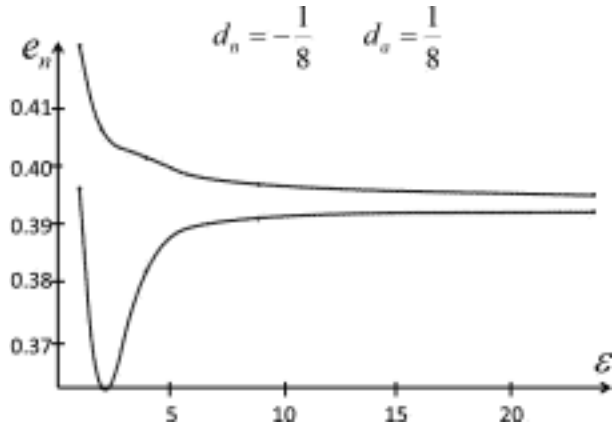


Fig. 5. As  $\varepsilon$  increases, the last contact figure  $e_n$  (lower curve) first decreases and then increases slowly; on the contrary, for the last one-member series  $e_n$  decreases continually. Both curves tend to the same point, i. e., the last contact figure is at the same time the last one-member series.

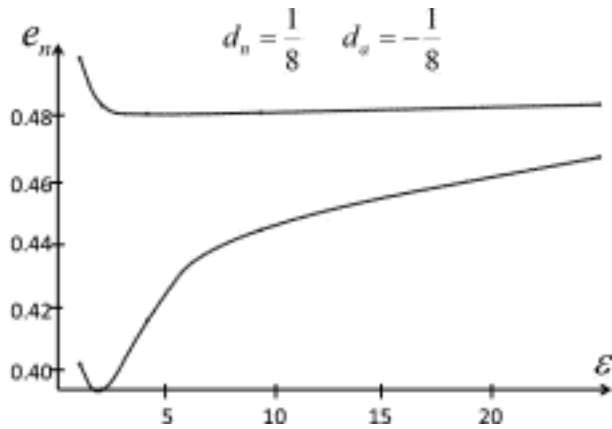


Fig. 6. As  $\varepsilon$  increases, the last contact figure  $e_n$  (lower curve) first decreases and then increases slowly; on the contrary, last one-member series  $e_n$  decreases continually. Both curves tend to the same point, i. e., last contact figure is at the same time last one-member series.

5.3. Consequences of the  $\varepsilon$ -value

To study the  $\varepsilon$  impact on our series, we assumed values for the parameters according to

$$e_1 = \frac{1}{2}, d_n = -\frac{1}{8}, \frac{1}{8}, d_a = \frac{1}{8}, -\frac{1}{8}, \varepsilon = 1, 2, 4, 9, 24,$$

and constructed the series changing  $e_a$  for a given  $e_n$  of a set  $0.1 \dots 0.5$ , as formerly done. As an illustration, only cases  $d_n = \mp 1/8, d_a = \pm 1/8$  were con-

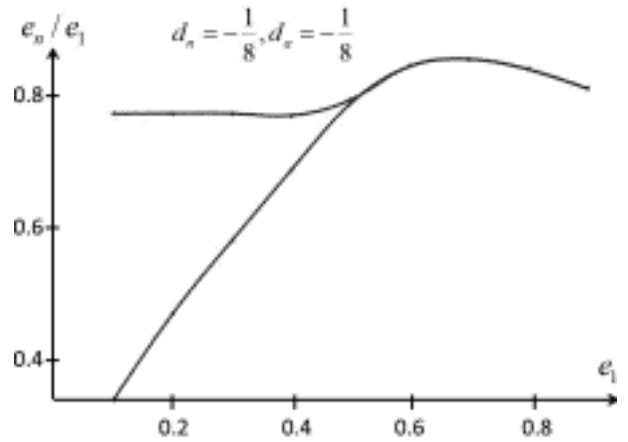


Fig. 7. As  $e_1$  increases, the last contact figure  $e_n/e_1$  (lower curve) increases continuously, practically for all  $e_1$  values; on the contrary, for the last one-member series  $e_n/e_1$  remains constant up to about  $e_1 = 0.5$ . Both curves coincide after about  $e_1 = 0.5$ . The curves were plotted for  $d_n, d_a = -1/8$ .

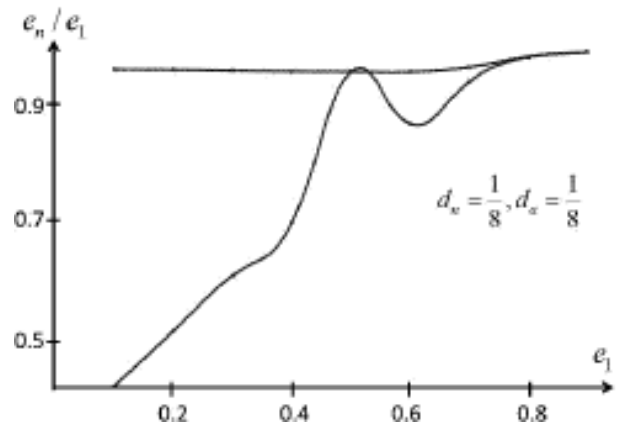


Fig. 8. As  $e_1$  increases, the last contact figure  $e_n/e_1$  (lower curve) increases continuously with some small oscillation, for all  $e_1$  values; on the contrary, the last one-member series  $e_n/e_1$  remains constant ( $\approx 0.98$ ) practically all the way. Both curves coincide after about  $e_1 = 0.7$ . The curves were plotted for  $d_n, d_a = 1/8$

sidered, and cases with  $d_n = d_a = -1/8, 1/8$  were disregarded. We refer briefly to these  $d$ -values as  $-+, +- , --, ++$  (first sign for  $d_n$ , second for  $d_a$ ). Generally speaking, we did not find any new property, (other than those recognized above) when  $\varepsilon$  was modified, i. e., for each  $\varepsilon$ , the set of series can or cannot show angular velocity distribution ‘turning points’ (transition to monotonically increasing distri-

bution), there is a final series having a contact figure, and there is a last (one-member) series. Clearly, as  $\varepsilon$  changes, the values characterizing a last contact figure, a last series, and a transition figure, must suffer modifications. The contact limiting figure has an  $e_n$ -value that first decreases and then increases, as  $\varepsilon$  increases from 1 to 24 (see Figure 5). On the other hand,  $e_n$  in the last series continually decreases as  $\varepsilon$  increases. The  $e_n$  span between last contact figure series and last series initially increases and thereafter continuously decreases (Figure 5).

#### 5.4. Consequences of the $e_1$ -value

To study changes of our basic series (Figure 2) regarding the nucleus and atmosphere relative size  $e_1$ , we varied it in steps of 0.1 from 0.9 down. We fixed  $d_a = \pm 1/8$ ,  $d_n = \pm 1/8$ ,  $\varepsilon = 1$  and constructed  $e_n$  series varying  $e_a$  for each  $e_1$  value of the set. For example, when  $e_1 = 0.9$  we built the series for  $e_n = 0.1, 0.2, \dots$ . Qualitatively again, we found series with or without transition limits,  $e_a$  upper limits, last contact figure for  $e_n$  series, and final one-member series. Quantitatively, there are differences regarding the above results. The  $\omega^2$  magnitudes and the variation range change; the  $e_n$  gap between last contact figure and last one-member series grows as

$e_1$  decreases, starting at  $e_1 = 0.5$ ; likewise, beyond  $e_1 = 0.5$  the gap approaches 0 (see Figures 6 and 7). This behavior is somewhat similar to the  $\varepsilon$ -effect (Figures 4 and 5): as  $e_1$  or  $\varepsilon$  increases the gap becomes narrower, and finally it disappears.

We thank Edgardo Ugalde Saldaña from the Instituto de Física UASLP, Mexico, for kindly providing computer support that facilitated the calculations of our numerical results.

#### REFERENCES

- Chandrasekhar, S. 1969, *Ellipsoidal Figures Of Equilibrium* (New Haven, CT: YUP)
- Cisneros, J. U., Martínez, F. J., & Montalvo, J. D. 2015, *RMxAA*, 51, 119
- \_\_\_\_\_. 2015, *RMxAA*, 51, 253
- Dryden, H. L., Murnaghan, F. P. & Bateman, H. 1956, *Hydrodynamics* (Dover Publications Inc.)
- Jeans, J. H. 1919, *PhilTrans.R.Soc.*, (Cambridge: Cambridge University Press)
- Lyttleton, R.A. 1953, *The Stability of Rotating Liquid Masses*, (Cambridge: MA:CUP) 37
- Montalvo J. D., Martínez, F. J. & Cisneros, J. U. 1983, *RMxAA*, 5, 293

Joel U. Cisneros Parra: Facultad de Ciencias, Universidad Autónoma de San Luis Potosí, Zona Universitaria s/n, San Luis Potosí, S.L.P., México (cisneros@galia.fc.uaslp.mx).

Francisco J. Martínez Herrera and J. Daniel Montalvo Castro: Instituto de Física, Universidad Autónoma de San Luis Potosí, Zona Universitaria s/n, San Luis Potosí, S.L.P., México.